ISSN 1392-1320 MATERIALS SCIENCE (MEDŽIAGOTYRA). Vol. XX, No. X. 2026

Transmittance Spectrum Analysis of a (SiO_2/TiO_2) One-dimensional Defective Photonic Crystal Structure for some Human Blood Compound Sensing

Ahlam AOUACHIR [1]*, Khalfallah BENBELGACEM [1, 2], Kamal Eddine AIADI [1], Omar BENTOUILA [1], Anfal BENREZKALLAH [1]

[1] *LENREZA Laboratory, Physics Department, University Kasdi Merbah Ouargla, 30000, Ouargla, Algeria*
[2] *LRPPS Laboratory, Physics Department, University Kasdi Merbah Ouargla, 30000, Ouargla, Algeria*

http://doi.org/10.5755/j02.ms.41000

Received 28 March 2025; accepted 30 May 2025

This study aims to investigate the transmittance spectrum of a one-dimensional photonic crystal 1D-PhC biosensor composed of SiO_2/TiO_2 multilayers for real-time detection of human blood components in the visible wavelength range. The Transfer Matrix Method (TMM) implemented in Python was employed to derive the transmittance spectrum of the sensor. The proposed sensor effectively detects shifts in the transmittance profile of four selected blood compound indices (blood plasma, white blood cells, hemoglobin, and red blood cells) within the photonic band gap (PBG) of wavelength between 650 – 1050 nm and 2170 nm thickness of the defect layer using seven periodic layers of TiO_2/SiO_2 and a 20° incident theta angle. A parametric analysis was conducted by varying the defect layer thickness d_0, the number of periodic layers N, and the incidence angle θ_i to optimize the sensor performance. At d_0 = 10D and N = 7, the optimized sensor design consistently detected subtle changes in the refractive index caused by hemoglobin level fluctuations, maintaining high sensitivity and quality factors across various concentrations.
Keywords: SiO_2/TiO_2, 1D photonic crystal, VIS wavelength, human blood, biosensor, transfer matrix method.

1. INTRODUCTION

The concentration ratios, values, and conditions of human blood components serve as critical indicators of an individual's health status, reflecting the physiological state of tissues and organs throughout the body. Any deviations from normal blood composition can disrupt physiological balance and adversely affect overall health [1, 2]**.** This biological fluid is composed primarily of three types of cells: red blood cells, which transport oxygen and carbon dioxide; white blood cells, which are integral to the immune response; and platelets, which facilitate clotting to prevent excessive bleeding [3, 4, 5]. These cellular components are suspended in plasma, the liquid matrix of blood, which plays a vital role in transporting nutrients, waste products, proteins, hormones, and antibodies. Each blood component fulfills a specific function, and its precise regulation is essential for maintaining optimal health [6, 7].

Despite the wide range of methodologies and techniques available for the quantification of biochemical markers and human biofluids, there remains a pressing need for cost-effective and reliable biosensors for real-time detection in healthcare and medical applications [8, 9, 10]. In light of increasing interest and advancements in biochemical detection, photonic crystal biosensors offer a promising solution [11, 12]. Various configurations of sensors based on photonic crystal (PhC) structures have demonstrated significant advantages not only in biosensing but also in temperature, pressure, and chemical detection applications [13, 14, 15], making them attractive for commercial and clinical use**.** These sensors leverage the unique optical properties of photonic crystals to achieve high sensitivity and selectivity in detecting biomolecules, paving the way for innovative applications in medical diagnostics and environmental monitoring**.** Among these, one-dimensional photonic crystal (1D-PhC) structures stand out due to their lower fabrication costs and reduced optimization parameters compared to their two-dimensional and three-dimensional counterparts [16, 17].

Although refractive index (RI) sensing is a well-established method in the field of biosensing, most existing studies focus on general-purpose detection without targeting specific blood biomarkers or optimizing sensor design for narrow spectral sensitivity. There is a noticeable gap in understanding how defective 1D-PhCs composed of SiO_2 and TiO_2 can be engineered in the visible wavelength range (VIS) to achieve precise detection of specific blood components, particularly under biologically relevant conditions. This study addresses that gap by proposing and optimizing a 1D-PhC biosensor structure capable of detecting subtle RI changes corresponding to hemoglobin concentration and related blood abnormalities, thereby advancing the clinical applicability of photonic sensors.

Previous studies have indicated that photonic crystals can be engineered to exhibit specific optical characteristics, making them advantageous for a wide range of sensing applications, including biosensing. However, there is limited understanding of how defective one-dimensional photonic crystals composed of SiO_2 and TiO_2 can be optimized in the visible range for sensing specific components of human blood. The present study aims to analyze the transmittance spectrum of a defective 1D-PhC composed of these two selected materials, silicon dioxide

* Corresponding author: A. Aouachir
E-mail: *aouachir.ahlem@univ-ouargla.dz*

(SiO_2) and titanium dioxide (TiO_2) and evaluate its effectiveness for sensing key blood components.

To achieve this goal, this paper is organized as follows: following this brief introduction, which underscores the importance of the topic and its associated challenges, Section 2 delineates the proposed sensor design and the methodology employed to simulate and analyze the transmittance spectrum. Section 3 presents a comprehensive analysis and discussion of the numerical results, emphasizing the impact of defect layer thickness (d_0), number of periodic layers (N), and incidence angle (θ_i) on sensor performance, while also validating the sensor's efficacy in detecting malaria. Finally, in Section 4, we present a summary of the results obtained in this study.

2. SENSOR DESIGN AND THEORETICAL FORMULATION

2.1. Sensor design

Several methods are used to design the *1D-PhC* biosensor, but in general, *1D-PhC* are made of two periodic stacked layers with different Refractive Index *RI* materials with a cavity in the middle [19, 20, 21], in order to obtain the structure of $(n_1\ n_2)^N C(n_1\ n_2)^N$, as shown in Fig. 1.

The periodic variation of *RI* in the multilayer structure inhibits the transmission of certain frequency bands in the transmission spectra, a phenomenon known as photonic band gap (PBG) [22, 23]. These PBG*s* significantly influence the optical properties of the multilayer structure, particularly in terms of light transmittance, reflectance, and absorption [24, 25].

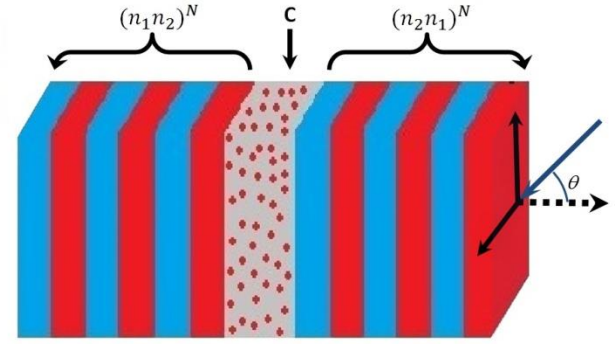

Fig. 1. Illustration of the designed *1D*-photonic crystal

For the present biosensor, the two selected materials were SiO_2 and TiO_2. SiO_2 has a three-dimensional structure in which each silicon atom is bonded to four oxygen atoms in a tetrahedral arrangement [26]. The amorphous structure of molten silicon leads to pure glassy properties characterized by the absence of impurities and defects, which results in high optical quality and low light absorption, with an *RI* given by [26]:

$$n_1{}^2(\lambda) = 1 + \frac{0.6961663\,\lambda^2}{\lambda^2 - 68404.3^2} + \frac{0.4079426\,\lambda^2}{\lambda^2 - 116241.4^2} + \frac{0.8974794\,\lambda^2}{\lambda^2 - 9896161^2}. \quad (1)$$

The second material is titanium dioxide *TiO_2*, a metal belonging to the tetragonal crystal system that exhibits high dispersion and high *RI*, which makes it useful in optical applications, where [27]:

$$n_2{}^2(\lambda) = 5.913 + \frac{244100}{\lambda^2 - 80300}. \quad (2)$$

The blood sample to be sensed is introduced into cavity *C* with thickness d_0, and the refractive indices of the four human blood components are: blood plasma $n(bp) = 1.35$, white blood component $n(bw) = 1.36$, hemoglobin $n(bh) = 1.38$, and red blood component $n(br) = 1.40$ [18]. The periodic layers on each side of cavity *C* are symmetric forms made of two different thicknesses d_1 and d_2.

According to the quarter-wave layer law $n_1\ d_1 = n_2\ d_2 = \lambda/4$ [28], the thickness of the SiO_2 layer is chosen as $d_1 = 138$ nm and $d_2 = 79$ nm for the TiO_2 layer, to obtain a central wavelength in *VIS* range $\lambda_c = 800$ nm, The defect layer thickness d_0 is defined as an integer multiple of the lattice period *D*, where $D = d_1 + d_2$ represents the combined thickness of one unit cell consisting of SiO_2 and TiO_2 layers in the 1D photonic crystal.

When the 1*D-PhC* structure is exposed to electromagnetic radiation, cavity *C* exhibits resonance frequency modes confined in the PBG, depending on the defect content and thickness [29]. The electromagnetic wave propagation through the structure was analyzed using the transfer matrix method TMM. This method aims to contain many interfaces separating different homogeneous layered media and obtain different optical properties of the system, such as reflection and transmission coefficients of waves at different frequencies [30, 31].

2.2. Transfer matrix method

The transfer matrix method is well-known in photonics for calculation and analysis of electric and magnetic field properties in stratified media, and it is widely used in the case of variable stresses in multilayer systems [32]. Exploiting this method we programmed an algorithm in Python to simulate the electromagnetic wave behavior in the system based on two key functions.

The first function calculates the *RI* for each medium within the system, Accordingly, we define it as follows:

$$\mathrm{Def}n_i(\lambda) = \begin{cases} n_0 = n_4 = 1 & \text{air} \\ n_1 & SiO_2 \\ n_2 & TiO_2 \\ n_3 & \text{blood components} \end{cases}. \quad (3)$$

The second function uses a 2 × 2 matrix to describe the boundary conditions of electric field vectors at different interfaces. According to TMM, the system matrix is formulated to calculate the transmission spectrum, as follows [32]:

$$M_{tot} = \begin{pmatrix} M_{11} & M_{12} \\ M_{21} & M_{22} \end{pmatrix} = D_o^{-1}(M_1M_2)^N M_3(M_1M_2)^N D_4\,, \quad (4)$$

where M_i is the transfer matrix for each layer, given by:

$$M_i = D_i P_i D_i^{-1}; i = 1,2,3., \quad (5)$$

where:

$$D_i = \begin{pmatrix} 1 & 1 \\ n_i\cos\theta_i & -n_i\cos\theta_i \end{pmatrix}. \quad (6)$$

For *S* wave polarization we have:

$$P_i = \begin{pmatrix} e^{i\phi_i} & 0 \\ 0 & e^{-i\phi_i} \end{pmatrix}, \ \phi_i = \frac{2\pi n_i}{\lambda} d_i cos\theta_i; \quad (7)$$

and

$$\theta_i = \sin^{-1}\left(\frac{n_{i-1}}{n_i}\sin\theta_{i-1}\right). \quad (8)$$

Here transmission coefficients will be given by:

$$t = \frac{1}{M_{11}}; \quad (9)$$

and the profile pattern of the transmittance of the structure is expressed by:

$$T = \frac{n_4}{n_0}\cos\theta_4 |t|^2. \quad (10)$$

To analyze the transmittance spectrum of the proposed sensor, we performed a parametric analysis by varying the defect layer thickness d_0, the number of layers N, and the incident angle θ_i. This analysis aimed to determine the quality factors of the sensor for each case to detect the four blood components. These factors include sensor sensitivity S and quality factor Q given by:

$$S = \frac{\lambda_{res}}{\Delta n}; \quad (11)$$

$$Q = \frac{\lambda_{max}}{\text{FWHM}}, \quad (12)$$

where $\Delta\lambda_{res} = \lambda_{max} - \lambda_{max_0}$, and $\Delta n = n - n_0$, using $n_0 = 1.33$ (water refraction index) as reference, λ_{max} is the peak maximum position, and FWHM is the full width at half maximum.

By adjusting d_0, N, and θ_i, we sought to optimize the sensor's ability to detect the four specific blood components. This approach enabled us to assess the S and Q of the sensors under various conditions, providing insights into their detection capabilities. The analysis focused on critical factors that determine the efficacy of the sensor. We examined λ_{max}, which indicates the wavelength at which the sensor exhibited the strongest response to the target blood components. Additionally, we evaluated the FWHM, which is a measure of the peak width that influences the resolution of the sensor and its ability to distinguish between closely spaced spectral features. By considering these parameters in conjunction with S and Q, we aim to identify the optimal configuration for the sensor, balancing the detection accuracy and overall performance in blood component detection.

3. RESULTS AND DISCUSSION

3.1. Effect of the defect layer thickness

Fig. 2 presents distinct transmittance spectra patterns within the photonic band gap (PBG) for varying defect layer thicknesses. At $d_0 = 2D$, a single transmission peak appears for each of the four blood components, indicating simple resonant interactions. Increasing the thickness to $d_0 = 4D$ results in two peaks per component, reflecting the emergence of more complex optical resonances. To capture the full evolution of these resonances and the development of the PBG, a broad wavelength range (300 – 1500 nm) was chosen for Fig. 2, ensuring that all relevant spectral features are visible. Further increasing the defect thickness to $d_0 = 10D$ leads to five distinct peaks for each component.

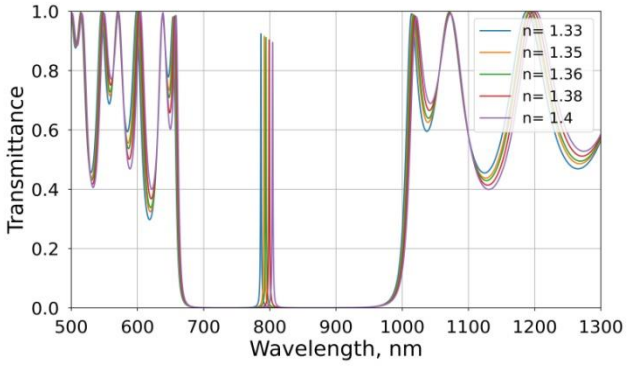

a

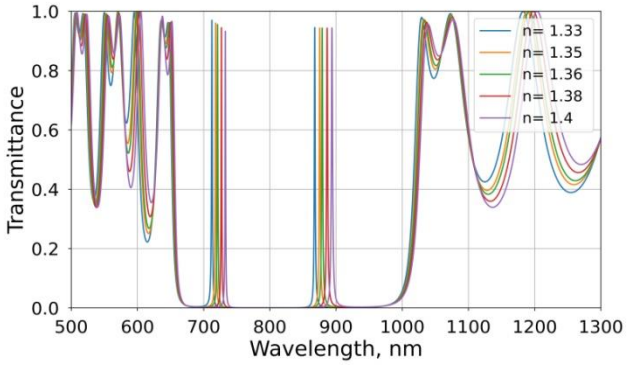

b

Fig. 2. Variation in transmittance spectra with different defect layer thicknesses d_0: a – $d_0 = 2D$; b – $d_0 = 4D$

These results demonstrate that greater defect layer thickness introduces additional resonant modes within the PBG. This behavior aligns with previous studies, which show that thicker defect layers extend the optical path and enhance light-matter interactions, thereby generating more complex transmittance spectra [30, 33]. However, the increasing number of peaks also made them more difficult to distinguish, presenting challenges for practical sensing applications. Therefore, no further simulations were conducted beyond a defect thickness of $d_0 = 10D$.

A decrease in the FWHM of the peaks was observed as d_0 increased (Table 1). The narrow peaks resulted from enhanced constructive interference and reduced damping, which improved the resolution of the sensor. The decrease in FWHM corresponds to an increase in Q (Eq. 12). The configurations with $d_0 = 6D$, $9D$, and $10D$ exhibited particularly high quality values, with $Q = 1775.02$ and $S = 457.8$ for peaks near the central wavelength λ_c. The peaks at these thicknesses were more distinct and sharper, suggesting enhanced sensor sensitivity in detecting minute alterations in the refractive index (RI) of the blood sample.

3.2. Effect of layers number

The impact of the number of layers (N) on sensor efficiency was explored through a detailed analysis of transmittance spectra for N values of 3 and 5 (Fig. 3). With the thickness set at $d_0 = 2D$ and the incidence angle of $0°$,

the study revealed notable differences in peak profiles and interference patterns.

Table. 1. Peak profile factors for the four blood components in the case of different defect layer thicknesses d_0

Cavity d_0	Blood plasma	White blood cells	Hemoglobin	Red blood cells	Peak factors
4D	718.16	721.04	726.89	732.83	λ_{max} nm
	1.26	1.21	1.11	1.04	FWHM nm
6D	786.77	790.79	798.85	806.93	λ_{max} nm
	0.65	0.65	0.67	0.69	FWHM nm
9D	808.52	813.14	822.38	831.61	λ_{max} nm
	0.51	0.52	0.56	0.59	FWHM nm
10D	785.00	789.58	798.76	806.94	λ_{max} nm
	0.44	0.44	0.45	0.47	FWHM nm

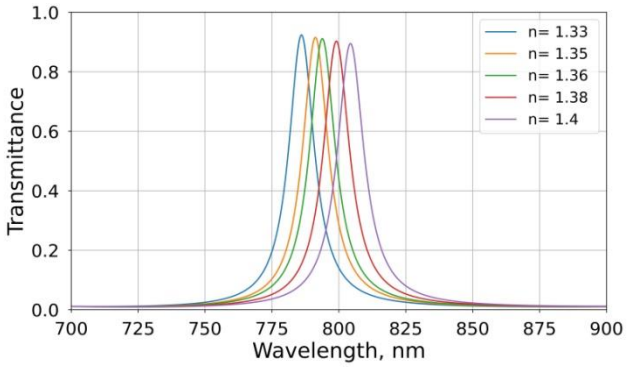

a

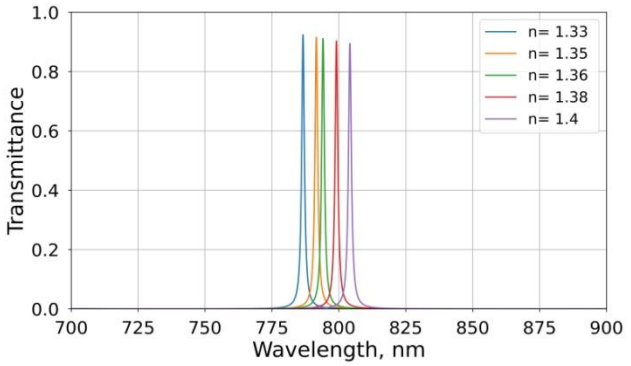

b

Fig. 3. Variation in transmittance spectra with different number of layers N: a – N = 3, b – N = 5

As the number of layers increased, the peaks became more pronounced and sharper, while the interference between peaks decreased. This trend suggests that sensors with a higher number of layers possess enhanced sensitivity in detecting subtle variations in the refractive index of blood components. The transmittance spectrum for the seven-layer configuration N = 7 demonstrated particularly promising results. A significant reduction in the full width at half maximum FWHM of the peaks was observed, indicating improved spectral resolution and potentially greater precision in measurements (Table 2). These results are in good agreement with those reported in the scientific literature [19, 34]. This enhancement in spectral characteristics could lead to more accurate and reliable detection of specific blood components or biomarkers. The findings underscore the importance of optimizing the number of layers in sensor design to achieve the desired balance between sensitivity and practical implementation, as increasing the number of layers may also introduce additional complexity and manufacturing challenges.

Table. 2. Peak profile factors for the four blood components in the case of different number of layers

Number of layers	Blood plasma	White blood cells	Hemoglobin	Red blood cells	Peakfactors
N = 3	791.22	793.83	799.07	804.34	λ_{max} nm
	11.69	11.78	11.98	12.19	FWHM nm
N = 5	791.59	794.08	799.10	804.13	λ_{max} nm
	1.23	1.23	1.23	1.28	FWHM nm
N = 7	791.63	794.11	799.10	804.11	λ_{max} nm
	0.13	0.12	0.13	0.14	FWHM nm

Additionally, in (Table 2) for FWHM = 0.14 nm and $\lambda_{max} = 791.63$ nm the Q and S factors significantly increased, and reaching 6000 and 247.5 respectively for N = 7, indicating enhanced resolution and performance, thereby improving the sensor efficiency.

3.3. Effect of incident wave angle

The impact of the incident wave angle θ_i on the sensor was examined with fixed structural properties at $d_0 = 2D$ and N = 5 using angles of incidence of 0°, 10°, and 20°. As the angle increased, the transmittance spectrum shifted to shorter wavelengths and the peaks moved to the visible range, as illustrated in (Fig. 3 b and Fig. 4).

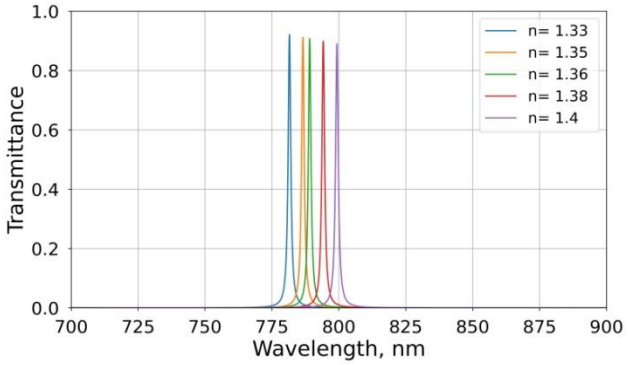

a

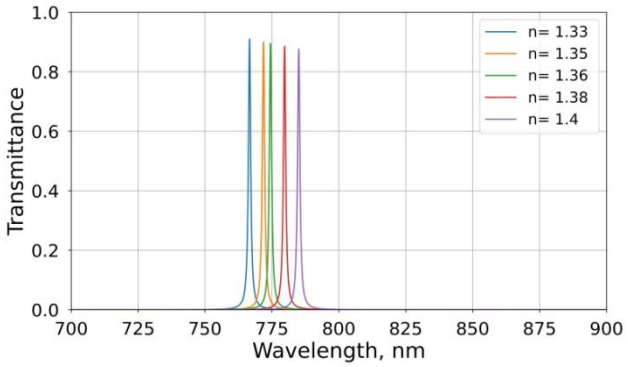

b

Fig. 4. Variation in transmittance spectra with differ incident wave angle θ_i: a – $\theta_i = 10°$; b – $\theta_i = 20°$

This behavior is consistent with observations reported in studies [21, 35]. This demonstrates that the resonance modes within the PBG were significantly affected by the angle of incidence. Additionally, a decrease in the FWHM was noted at higher incidence angles, resulting in sharper peaks (Table 3). The *S* and *Q* factors also increase with θ_i, allowing more accurate measurements. However, the effects of varying θ_i on *S* and *Q* were less significant than those caused by variations in d_0 and *N*. Adjustments in d_0 and *N* had substantial effects on the transmission spectrum, leading to enhanced changes in PBG width and improved *S* and *Q* factors.

Table. 3. Peak profile factors for the four blood components in the case of different incident wave angle θ_i

Incident wave angle θ_i	Blood plasma	White blood cells	Hemog-lobin	Red blood cells	Peak factors
$\theta_i = 0°$	791.59	794.08	799.10	804.13	λ_{max} nm
	1.23	1.23	1.25	1.28	FWHM nm
$\theta_i = 10°$	786.57	789.09	794.17	799.27	λ_{max} nm
	1.16	1.17	1.19	1.22	FWHM nm
$\theta_i = 20°$	771.84	774.46	779.72	785.01	λ_{max} nm
	1.00	1.01	1.02	1.04	FWHM nm

3.4. Validation of the designed sensor's efficacy

To validate the proposed sensor, the results reported by Saini, S. K., & Awasthi, S. K. (2023) [36] were utilized prior to conducting the performance analysis under specified hemoglobin concentrations of five malaria-infected blood cell types (See Table 4).

Considering the optimization of sensor parameters for optimal performance with N = 7, θ_i=20°, and $d_0 = 10D$, we assessed the device's efficiency by varying the concentration of hemoglobin (C_{HB}) within the blood cells. The correlation between hemoglobin concentration and the RI of the sample is represented by the following formula [33]:

$$C_{HB} = 402.35 n_{RBC} - 535.8. \quad (13)$$

Fig. 5 presents the transmission spectrum of the five types of infected blood cells. These results indicate that minimal variations in hemoglobin concentration have slightly affected the clarity of the transmission spectrum peaks. Furthermore, the differentiation between the peaks was distinct, and these changes did not significantly affect the *S* and *Q* values of the sensor.

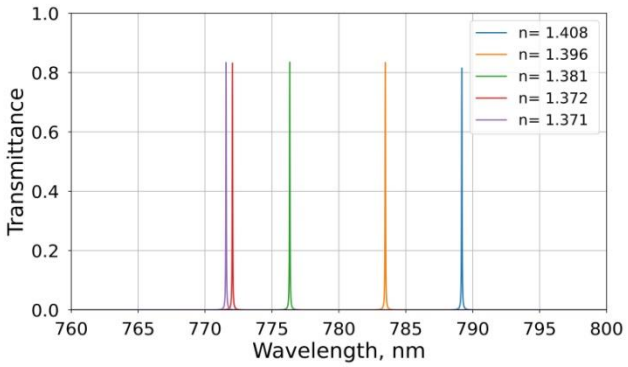

Fig. 5. Transmittance variation at different hemoglobin concentrations levels of different blood cells

Table 4 categorizes the sensor's performance data across different hemoglobin concentrations and compares them with the results of Saini, S.K., and Awasthi, S.K. [36]. The findings demonstrate that *S* is minimally affected by the RI, ranging from 476.1 to 476.7, indicating the stability of the discrimination between the peaks for each concentration. This value is higher than the result obtained by Saini, S.K., and Awasthi, S.K. [36], which is estimated at 327.70. The stability also refers to the device's ability to accurately detect differences in hemoglobin concentration despite the low *Q* value compared to the work of Saini, S.K., and Awasthi, S.K. [36]; however, it remains an acceptable quality factor for the sensor. This outcome confirmed the reliability of the device. High *S* factors indicate the sensor's ability to maintain accuracy and reliability in detecting RI variations resulting from changes in the hemoglobin levels of different blood cells.

4. CONCLUSIONS

In conclusion, the proposed one-dimensional photonic crystal biosensor, composed of alternating layers of SiO_2 and TiO_2, demonstrates strong potential for the precise detection of blood components. Transmittance spectrum analysis revealed high sensitivity to slight variations in the refractive index within the 0.01 – 0.02 range, confirming the sensor's responsiveness to subtle biochemical changes. The sensor's sensitivity and quality factor were notably enhanced by increasing both the defect layer thickness and the number of periodic layers.

Table. 4. Comparison of sensitivity, quality factor, λ_{max} and FWHM values of proposed 1*D-PhC* sensor for malaria sensing and detection with similar work by Saini, S.K., and Awasthi, S.K. (2023) [36]

Hemoglobin concentration C_{HB}	Cell A 30.900 g/dL	Cell B 25.599 g/dL	Cell C 19.789 g/dL	Cell D 16.289 g/dL	Cell E 15.990 g/dL
RI	1.408	1.396	1.381	1.372	1.371
λ_{max} (Saini, S. K et al) [36]	671.40	667.80	662.70	659.60	659.20
λ_{max} (current work)	789.19	783.47	776.33	772.05	771.57
FWHM (Saini, S. K et al) [36]	0.11	0.036	0.0135	0.01	0.0095
FWHM (current work)	0.03	0.02	0.03	0.03	0.03
S (Saini, S. K et al) [36]	–	300.00	322.20	327.70	310.50
S (current work)	–	476.67	476.30	476.11	476.22
Q (Saini, S. K et al) [36]	6103.63	18550.00	49088.80	65960.00	69389.47
Q (current work)	26306.33	39173.50	25877.67	25735.00	25719.00

A strong correlation was observed between the defect layer thickness and sensitivity, with optimal performance achieved at d_0 = 2170 nm. Increasing d_0 introduced multiple peaks within the photonic bandgap, while also sharpening peak profiles, thereby improving detection accuracy. Notably, when the cavity thickness equaled ten times the lattice period ($D = d_1 + d_2$), the sensor achieved S and Q values of 476.67 and 39,173, respectively.

Increasing the number of layers also helped reduce peak overlap, resulting in narrower transmission peaks and a higher *Q* factor. The optimized structure (N = 7, $d_0 = 10D$) consistently detected subtle RI changes associated with varying hemoglobin concentrations, maintaining high sensitivity and signal stability across a range of blood conditions.

Furthermore, the sensor effectively distinguished hemoglobin concentration variations in different types of infected blood cells. Despite slight variations in refractive index, the sensor exhibited stable sensitivity (S) and acceptable *Q* factor values, with consistent peak differentiation. While the *Q* factor is somewhat lower compared to select existing designs, it remains sufficient for reliable detection.

These results highlight the sensor's promise for clinical applications in hematology, particularly for monitoring hemoglobin levels and identifying blood disorders. Future research may focus on optimizing the *Q* factor and evaluating performance in more complex biological environments to further enhance diagnostic utility.

REFERENCES

1. **Poletaev, A.** Composition of the Blood and Reflection of the Health State of Human Body *Biomedical and Pharmacology Journal* 11 (4) 2018: pp. 1797 – 1800. https://doi.org/10.13005/bpj/1551
2. **Yurkovich, J.T., Hood, L.** Blood Is a Window into Health and Disease *Clinical Chemistry* 65 (10) 2019: pp. 1204 – 1206. https://doi.org/10.1373/clinchem.2018.299065
3. **Bain, B.J.** Structure and Function of Red and White Blood Cells and Platelets *Medicine* 49 (4) 2021: pp. 183 – 188. https://doi.org/10.1016/j.mpmed.2021.01.001
4. **Humphry, E., Armstrong, C.E.** Physiology of Red and White Blood Cells *Anaesthesia & Intensive Care Medicine* 23 (2) 2022: pp. 118 – 122. https://doi.org/10.1016/j.mpaic.2019.01.001
5. **Page, M.J., Pretorius, E.** Platelet Behavior Contributes to Neuropathologies: A Focus on Alzheimer's and Parkinson's Disease *Semin Thromb Hemost* 48 (03) 2022: pp. 382 – 404. https://doi.org/10.1055/s-0041-1733960
6. **Sturkie, P.D., Griminger, P.** Blood: Physical Characteristics, Formed Elements, Hemoglobin, and Coagulation. In: *Sturkie, P. D.* (Ed.) *Avian Physiology* Springer 1976: pp. 53 – 75. https://doi.org/10.1007/978-3-642-96274-5_3
7. **Poletaev, A., Trukhanov, A., Grechko, A.** Molecular Composition of Blood Plasma and Condition of Human Organism at the Normal and Pathological State *Physical and Rehabilitation Medicine Medical Rehabilitation* 1 (2) 2019: pp. 37 – 42. https://doi.org/10.36425/2658-6843-19185
8. **Kumar, A.M., Kachhawa, K.** Biomedical Applications of Bioelectrochemical Sensors *Multifaceted Bio-sensing Technology* Academic Press 2023: pp. 239 – 260. https://doi.org/10.1016/B978-0-323-90807-8.00014-2
9. **Haleem, A., Javaid, M., Singh, R.P., Suman, R., Rab, S.** Biosensors Applications in Medical Field: A Brief Review *Sensors International* 2 2021: pp. 100100. https://doi.org/10.1016/j.sintl.2021.100100
10. **Kavitha, B.S., Pant, S., Sood, A.K., Asokan, S.** Fiber Grating Sensors and their Recent Applications in Biomedical Domain *Journal of Optics* 25 (8) 2023: pp. 084001. https://doi.org/10.1088/2040-8986/25/8/084001
11. **Heidari, P.F., Rahimi, F., Olyaee, Z.** Two-Dimensional Photonic Crystal Biosensors: A Review *Optics & Laser Technology* 144 2021: pp. 107397. https://doi.org/10.1016/j.optlastec.2021.107397
12. **Inan, H., Poyraz, M., Inci, F., Lifson, M.A., Baday, M., Cunningham, B.T., Demirci, U.** Photonic Crystals: Emerging Biosensors and Their Promise for Point-of-Care Applications *Chemical Society Reviews* 46 (2) 2017: pp. 366 – 388. https://doi.org/10.1039/C6CS00206D
13. **Chaudhary, V.S., Kumar, D., Pandey, B.P., Kumar, S.** Advances in Photonic Crystal Fiber-Based Sensor for Detection of Physical and Biochemical Parameters – A Review *IEEE Sensors Journal* 23 (2) 2022: pp. 1012 – 1023. https://doi.org/10.1109/JSEN.2022.3222969
14. **Srivastava, S.K.** Design of Temperature Sensor Based on One-Dimensional Photonic Crystal Containing Si–BGO Layer *Materials Open* 1 2023: pp. 2350003. https://doi.org/10.1142/2350003
15. **Ameen, A.A., Panda, A., Mehaney, A., Almawgani, A.H.M., Pradhan, D.D., Ali, G.A., Ali, Y.A.A., Elsayed, H.A.** An Investigation of High-Performance Pressure Sensor Employing a Polymer-Defect-Based 1D Annular Photonic Crystal *Photonics* 10 (7) 2023: pp. 731. https://doi.org/10.3390/photonics10070731
16. **Sadykov, A.I., Kushnir, S.E., Sapoletova, N.A., Napolskii, K.S.** One-dimensional Photonic Crystals Based on Anodic Titanium Oxide with a High Q Factor *Journal of Surface Investigation: X-ray, Synchrotron and Neutron Techniques* 14 2020: pp. 42 – 46. https://doi.org/10.1134/S1027451020010147
17. **Hassan, A.K.S., Mohamed, A.S., Maghrabi, M.M., Rafat, N.H.** Optimal Design of One-Dimensional Photonic Crystal Filters Using Minimax Optimization Approach *Applied Optics* 54 (6) 2015: pp. 1399 – 1409. https://doi.org/10.1364/AO.54.001399
18. **Mohammed, N.A., Hamed, M.M., Khalaf, A.A.M., Alsayyari, A., El-Rabaie, S.** High-sensitivity Ultra-quality Factor and Remarkable Compact Blood Components Biomedical Sensor Based on Nanocavity Coupled Photonic Crystal *Results in Physics* 14 2019: pp. 102478. https://doi.org/10.1016/j.rinp.2019.102478
19. **Abd El-Aziz, O.A., Elsayed, H.A., Sayed, M.I.** One-Dimensional Defective Photonic Crystals for the Sensing and Detection of Protein *Applied Optics* 58 (30) 2019: pp. 8309 – 8315. https://doi.org/10.1364/AO.58.008309
20. **Daher, M.G.** Supersensitive Biosensor Based on a Photonic Crystal Nanostructure for Blood Sugar Level Monitoring with

Ultra-High Quality Factor and Low Detection Limit *Optik* 275 2023: pp. 170581. https://doi.org/10.1016/j.ijleo.2023.170581

21. **Elsayed, H.A., Mehaney, A.** Theoretical Verification of Photonic Crystals Sensor for Biodiesel Detection and Sensing *Physica Scripta* 95 (8) 2020: pp. 085507. https://doi.org/10.1088/1402-4896/aba123
22. **Fu, L., Lin, M., Liang, Z., Wang, Q., Zheng, Y., Ouyang, Z.** The Transmission Properties of One-Dimensional Photonic Crystals with Gradient Materials *Materials* 15 (22) 2022: pp. 8049. https://doi.org/10.3390/ma15228049
23. **Mbakop, F.K., Falama, R.Z., Wu, F., Ayang, A., Essiane, S.N., Leontie, L., Djongyang, N., Iacomi, F.** Angular Dependence of Photonic Band Gap and Omni-Directional Reflection in One-Dimensional Photonic Crystal Applied to a Thermophotovoltaic Device *Results in Optics* 14 2024: pp. 100594. https://doi.org/10.1016/j.rio.2024.100594
24. **Zhang, H.F., Liu, S.B., Chen, Y.Q.** Properties of Photonic Band Gaps in Superconductor Multilayer Structure with Periodically Varying Ambient Temperature *Journal of Superconductivity and Novel Magnetism* 26 2013: pp. 2911 – 2917. https://doi.org/10.1007/s10948-013-2145-6
25. **Fu, L., Lin, M., Liang, Z., Wang, Q., Zheng, Y., Ouyang, Z.** The Transmission Properties of One-Dimensional Photonic Crystals with Gradient Materials *Materials* 15 (22) 2022: pp. 8049. https://doi.org/10.3390/ma15228049
26. **Refractive Index Database.** SiO2 Optical Properties. Available at: https://refractiveindex.info/?shelf=main&book=SiO2&page=Malitson
27. **Refractive Index Database.** TiO2 Optical Properties. Available at: https://refractiveindex.info/?shelf=main&book=TiO2&page=Devore-o
28. **Wu, C.J., Rau, Y.N., Han, W.H.** Enhancement of Photonic Band Gap in a Disordered Quarter-Wave Dielectric Photonic Crystal *Progress In Electromagnetics Research* 100 2010: pp. 27 – 36. https://doi.org/10.2528/PIER09111610
29. **Lu, H., Shi, S., Li, D., Bo, S., Zhao, J., Mao, D., Zhao, J.** λ/20-thick Cavity for Mimicking Electromagnetically Induced Transparency at Telecommunication Wavelengths *Advanced Photonics* 6 (3) 2024: pp. 036001. https://doi.org/10.1117/1.AP.6.3.036001
30. **Aly, A.H., Zaky, Z.A., Shalaby, A.S., Ahmed, A.M., Vigneswaran, D.** Theoretical Study of Hybrid Multifunctional One-Dimensional Photonic Crystal as a Flexible Blood Sugar Sensor *Physica Scripta* 95 (3) 2020: pp. 035510. https://doi.org/10.1088/1402-4896/ab60f4
31. **Kumar, V., Suthar, B., Kumar, A., Kumar, V., Singh, K.S., Bhargva, A., Ojha, S.P.** Wave Transmission in Dispersive Si-Based One-Dimensional Photonic Crystal *Optics and Photonics Journal* 2 (2) 2012: pp. 237 – 241. https://doi.org/10.4236/opj.2012.223036
32. **Yeh, P., Hendry, M.** Optical Waves in Layered Media. American Institute of Physics, 1990.
33. **Aly, A.H., Elsayed, H.A., Malek, C.** Optical Properties of One-Dimensional Defective Photonic Crystal Containing Nanocomposite Material *Journal of Nonlinear Optical Physics & Materials* 26 (1) 2017: pp. 1750007. https://doi.org/10.1142/S0218863517500072
34. **Zaky, Z.A., Ahmed, A.M., Shalaby, A.S., Aly, A.H.** Refractive Index Gas Sensor Based on the TAMM State in a One-Dimensional Photonic Crystal: Theoretical Optimisation *Scientific Reports* 10 2020: pp. 9736. https://doi.org/10.1038/s41598-020-66427-6
35. **Abadla, M.M., Elsayed, H.A.** Detection and Sensing of Hemoglobin Using One-Dimensional Binary Photonic Crystals Comprising a Defect Layer *Applied Optics* 58 (36) 2019: pp. 8309 – 8315. https://doi.org/10.1364/AO.379041
36. **Saini, S.K., Awasthi, S.K.** Sensing and Detection Capabilities of One-Dimensional Defective Photonic Crystal Suitable for Malaria Infection Diagnosis from Preliminary to Advanced Stage: Theoretical Study *Crystals* 13 (1) 2023: pp. 128. https://doi.org/10.3390/cryst13010128